European Journal of Pharmaceutics and Biopharmaceutics 194 (2024) 36–48

Contents lists available at ScienceDirect

European Journal of Pharmaceutics and Biopharmaceutics

journal homepage: www.elsevier.com/locate/ejpb

Research paper

Combination techniques towards novel drug delivery systems manufacturing: 3D PCL scaffolds enriched with tetracycline-loaded PVP nanoparticles

Sumeyye Cesur *

Center for Nanotechnology & Biomaterials Application and Research (NBUAM), Marmara University, Turkey
Department of Metallurgical and Materials Engineering, Faculty of Technology, Marmara University, Turkey

ARTICLE INFO

Keywords:
3D Printing
Electrospraying
Nanoparticles
Scaffolds
Drug release modulation

ABSTRACT

Drug delivery systems based on synthetic and natural polymers offer a new approach with a capacity to control the release of bio-active agents within time. In this work, we present different designs of Polycaprolactone (PCL) 3D scaffolds containing Polyvinylpyrrolidone (PVP) nanoparticles that can store a hydrophilic drug. The drug delivery system, combined of PCL and PVP polymers fabricated by additive manufacturing, aims for a solution for longer and more stabled drug delivery carrier. The drug, planned to be released to the targeted area, is sprayed with the electrospray method inside PVP nanoparticles on the different layers of the fabricated PCL scaffolds 3D printing. This makes obtaining a layered and porous scaffold and drug-loaded nanoparticles within this structure easier. Obtained PCL scaffolds containing Tetracyclines (Tet) loaded PVP nanoparticles showed that drug encapsulation into the interlayer extended the release time and exhibited a controlled release profile for days. Moreover, produced scaffolds have good biocompatibility and no harmful effects. The combination of 3D scaffolds and drug-loaded nanoparticles aims to develop new functional scaffolds by targeting more efficient and longer-lasting drug delivery.

1. Introduction

The additive manufacturing, in which two or more materials come together and the structures are formed with a 3D printer, is a potential method for regenerative medicine for implants,stem cells delivery carriers in stem cellstransplantations, or controlled drug delivery carriers, [1–4 5]. To provide the desired duration and release kinetics of drugs, biocompatible polymer scaffolds should have optimal composition and structure In contrast to the duration and kinetics of the release, the structure of the polymer scaffold ensures that the therapeutic composition containing the active substance is protected in the body from drug release. The preservation of the active ingredient in the polymer prevents fluctuations in drug levels that can occur simultaneously with sequential and ad hoc drug administration. This condition, gains more importance as the drug content increases, aims to achieve a spatial-temporal release model specific to the treatment site in contrary to conventional drug release systems [6].

Sustained release of a hydrophilic drug from the hydrophobic polymer carrier might be difficult, and phase separation and splitting of the drug from the matrix may occur, causing sudden release of the active substance [7]. In a layered scaffold-drug delivery system the hydrophilic drug can be preserved in a hydrophilic polymer in a form of particles, and integrated into the hydrophobic scaffold allowing for a longer and more stable release. This kinf od system have many advantages since it can provide physical bonds between biological parts such as cells and scaffolds due to drug and polymer scaffolds cell retention capacity [8].

Tetracycline (Tet) is an antibiotic used in the prophylaxis and treatment of both human and animal infections against microorganisms such as gram-positive and gram-negative bacteria, protozoa, parasites, and mycoplasmas [9–11]. Tet, which has a versatile and changeable structure, has been used in the treatment of diseases for more than half a century now due to its chemical backbone that interact with the cellular target [12]. Basically, in the working mechanism of Tet antibiotic interfere with bacterial proteins by binding to them at the site of biosynthesis through the 30S subunit of the bacterial ribosome. The mechanism of action of tetracyclines makes it impossible for bacteria to attach tRNA and in consequence the inhibition of the development of the bacterial cell occurs.[11]. Tet is used clinically for bacterial dysentery

* Corresponding author at: Center for Nanotechnology & Biomaterials Application and Research (NBUAM), Marmara University, Turkey.
E-mail address: sumeyye.cesur@marmara.edu.tr.

https://doi.org/10.1016/j.ejpb.2023.11.022
Received 18 July 2023; Received in revised form 20 November 2023; Accepted 26 November 2023
Available online 28 November 2023

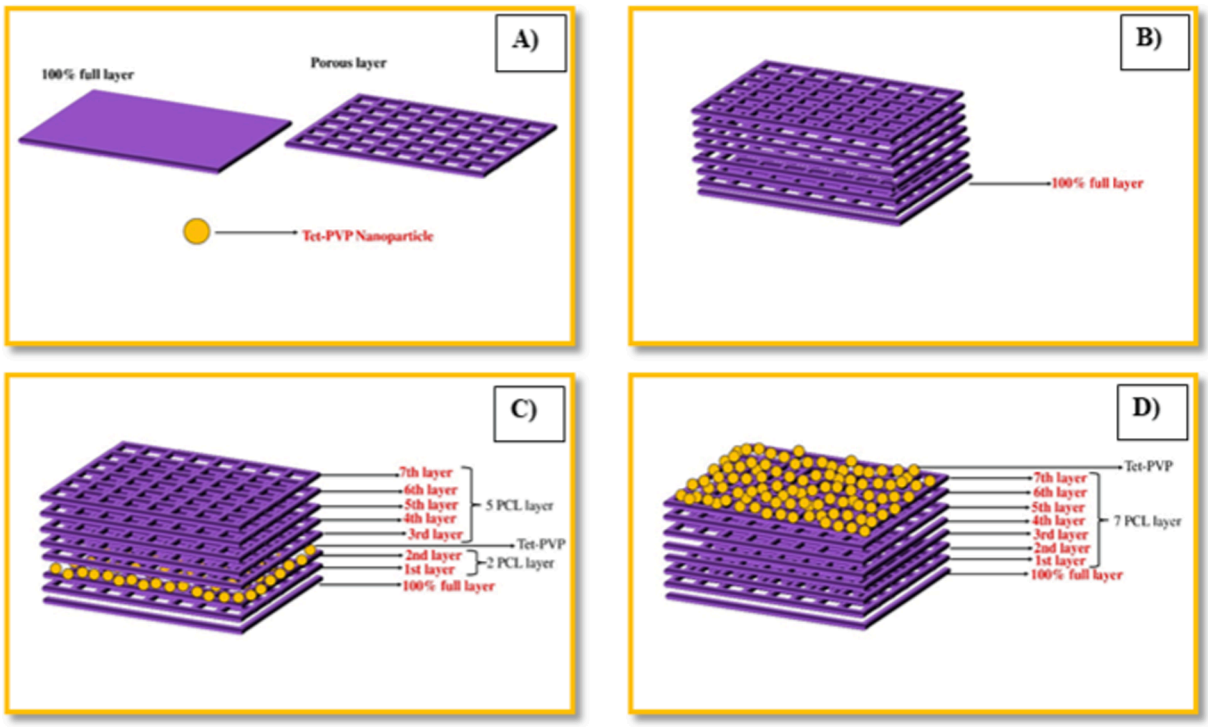

Fig. 1. A) The bottom layer is 100% PCL covered with the 3D method B) 7 pure porous layers on the 100 % PCL layer C) 2PCL/Tet-PVP/5PCL D) 7PCL/Tet-PVP.

[13], trachoma [14], pertussis [15], pneumonia [12], purulent meningitis [16], skin infections [17], and otitis media [18]. In the study of Karuppuswamy et al used PCLnanofibes enriched with Tet in different concentrations and tested the influence of the concentration of the drug on on the speed of tissue regeneration. The combination of PCL and Tet was found to be potential as a substrate for drug delivery carriers and scaffolds.

PCL is a low cost biodegradable, biocompatible, synthetic material, possessing good mechanical properties, that is satisfactory for many tissue engineering and drug delivery applications. On of the best methods to transform this polymer into scaffolds is 3D printing due to ease procesability and low melting temperature of the polymer. 3D printing is a very sufficient method for fabrication of complicated multilayer 3D structures with complex geometry and high porosity. Moreover, 3D scaffolds sustains micro-environments more accurately mimicking complex structure of the native tissues [19].

There are several techniques to produce nano- and microsized polymeric particles. These includes coacervation/precipitation, ionic gelation, spray drying, solvent evaporation, and electrospray.The electrospray method is an easy way to encapsulate drugs, and it can be performed in one step or multi-step process to produce the particles of desired sizes [20]. The electrospray technique can be utilized for advanced engineering application, and it allows to produce droplets of desired dimateres and morphologies from solutions or melts [21].

Polyvinylpyrrolidone (PVP) is one of the materials utilized for particles' matrix formation. It is a it is biocompatible, hemocompatible, low toxic, pH-stable polymers possessing high chemical and thermal resistance. Thanks to its special features the encapsulated active substance can be released in a controllable manner [22]. Guastaferro et al. obtained PVP particles with sizes of 140 ± 14 nm using electrospray for the development of rutin and quercetin with with antioxidant properties [2324]. Xu et al. used sodium alginate, polydopamine, and PVP to produce doxorubicin encapsulated particles using electrospraying to develop systems for cancer therapy. The studies have proven that the colloidal stability of the produced material is provided by PVP molecules, and the photothermal conversion efficiency of 27.4 % and antitumor therapeutic performance have been obtained [25]. Rose et al. used epirubicin hydrochloride drug adsorbed on the surface of magnetite (Fe3O4) nanoparticles coated and non-coated with PVP For selective cancer therapy. Results of the studies showed that nanoparticles coated with PVP were successful in killing tumor cells, showing 81 % growth inhibition [26].

In this study, polycaprolactone 3D scaffolds of different designs containing Polyvinylpyrrolidone nanoparticles, encapsulated with the hydrophilic drug Tet were fabricated. The influence of the scaffolds design and drug enrichment on the physical and chemical properties, drug release profiles, and *in vitro* cell viability were investigated. By combining 3D scaffolds and drug-loaded nanoparticles, it is aimed to design a safer, more controlled and more efficient drug delivery system, and to develop new functional scaffolds.

2. Materials and methods

2.1. Materials

Polycaprolactone (PCL, Mw:80000 g/mol), Polyvinylpyrrolidone (PVP, Mw ~ 1,300,000 g/mol), chloroform, ethanol and phosphate buffer saline (PBS, pH = 7.4) and Tetracycline (Tet) were provided by Sigma-Aldrich, (St. Louis, USA). The HFF-1 human fibroblast cells were acquired from the American Type Culture Collection (ATCC), and all *in vitro* tests were conducted using conventional sterile cell culture methods. 10 % fetal bovine serum (FBS), DMEM, and penicillin/streptomycin were purchased from Gibco (Thermo Fisher, Waltham, MA, USA). Thermo-Invitrogen provided the DAPI (4′,6-diamidino-2- phenylindole) staining kit.

2.2. Methods

2.2.1. Preparation of the PCL solution for 3D printing

17 wt% PCL was stirred in 10 ml of chloroform on a magnetic stirrer (Wise Stir®, MSH-20 Germany) for 2 h to form a transparent solution.

2.2.2. Preparation of PVP nanoparticles solution for use with the electrospray device

To obtain the nanoparticles, a solution of PVP with concentration of 13 wt% was first prepared. For this, 13 wt% PVP (1.3 g) was dissolved in 10 ml of ethanol and mixed until for fully dissolution at 25 °C. Then, 3 wt % (0.3 g) Tet was and mixed for about 1.5 h Further, the obtained yellow solution was transferred to the syringe to be electrospray and placed at a distance of 15 cm from the target. The production process of nanoparticles was performed with optimized operating paramaters: flow rate of0.3 ml/h and voltage of 12.5 kV.

2.2.3. Designing and production of the 3D printed scaffolds

Solid Works was used to design the 3D scaffold and was further converted to G-codes by slicing software (Simplify 3D). The scaffolds were designed to be square and their dimensions were 20 mm x 20 mm x 1 mm. Fabrication of the scaffolds was performed by employing a 3D printer (Hyrel 3D, SDS-5 Extruder, GA, USA). During printing a 10 ml syringe was loaded with PCL solutions, and printed through a 30 G needle, which was connected to the syringe. The printing parameters were as follows: fill pattern: linear, flow rate during the printing process: 1 ml/h, and printing speed: 10 mm/s.

2.2.4. Fabrication of PCL scaffolds of different designs containing Tet-loaded PVP

PVP particles were sprayed into different layers of the designed layered PCL scaffolds. For this, first a non-porous layer was printed as a base layer. For this, a thick-tipped needle is attached to the 3D printer. In design 1, on this layer, 2 layers of porous PCL layer are applied with a fine-tipped needle. The scaffold is transferred from the 3D printer to the electrospray machine, where Tet-loaded PVP nanoparticles are sprayed onto the two-layer polymer scaffold. After this process, the polymer scaffold is brought back to the same position in the 3D printer, and a 5-layer scaffold is applied on top of 2 layers with a fine- tipped needle, and a total of 7 layers are completed with a fine-tipped needle. In the other design 2, 7 layers of PCL layers are printed and drug-loaded PVP nanoparticles are sprayed on these 7 layers. In order not to lose efficiency during drug release, there is a gapless layer (100 % filled) on the bottom layer of all models. This common layer is the non-porous PCL scaffold In summary; Combination 1: 7-layer PCL/PVP particles (7PCL/PVP), Combination 2: 2-layer PCL/PVP particles/5-layer PCL (2PCL/PVP/5PCL), Combination 3: 7-layer PCL/Tet loaded-PVP particles (7PCL/Tet-PVP), Design 4: 2-layer PCL/Tet- loaded PVP particles/5-layer PCL (2PCL/Tet-PVP/5PCL) (Fig. 1).

2.2.5. Scanning electron microscopy (SEM)

Scanning Electron Microscopy (SEM, EVO LS 10, Zeiss) was used to investigate the surface morphologies porosity, diameter measurement, and particle distribution homogeneity of the particles and morphology and geometry of the scaffolds. Prior the observation under SEM all samples were sputter coated with gold (Au) and palladium (Pd) 120 s using sputter coater (Quorum SC7620, Laughton, UK). Diameter measurements were taken according to the image analysis performed with image analyzing software (Olympus AnalySIS, USA), and histogram graphs were drawn.

2.2.6. Fourier transform infrared spectroscopy analysis (FT-IR)

FTIR analysis (FTIR, Jasco, FT/IR 4700) was applied to investigate the molecular and chemical interactions within materials composing the scaffolds. For this analysis, samples were tested in a range of 450–4000 cm^{-1} at 4 cm^{-1} resolution and a scanning speed of 32 at room temperature.

2.2.7. Thermal behaviours of scaffolds

A Differential Scanning Calorimeter (DSC) device (Shimadzu, Japan) was used to determine characteristic temperatures of polymer transitions, such as glass transition temperature (Tg) and melting (Tm) point. Analysis was performed in temperature range of 25–300 °C and a heating rate of 10 °C/min.

2.2.8. Mechanical properties of the scaffold

A tensile test device (SHIMADZU, EZ-LX, China) was used to asses the mechanical properties of the scaffolds such as durability, flexibility, and resistance to rupture. The average thickness of the samples to be tested was measured from three different points with a digital micrometer (Mitutoyo MTI Corp., Aurora, CO, USA During the test the lower and upper edges of the scaffolds were positioned horizontally following the direction of implemented force.

2.2.9. Swelling and degradation behaviours of scaffolds

To measure the swelling capacity and degradability of the scaffolds, 4 days incubation and 18 days incubation in PBS was performed. Prioir the test, all samples were cut into equal weights and the dry weights (W0) of the samples were recorded using precision balance, and afterthe samples were transferred into Eppendorf tubes containing 2 ml of phosphate- buffered saline (PBS, pH 7.4).

During swelling measurements, the Eppendorf tube containing the samples in PBS was shaken at 37 degrees at 380 rpm. Wet weight (Ww) was measured daily for and swelling capacity was calculated according to the formula in Eq. (1) [27]

$$SD = \frac{W_w - W_0}{W_0} \cdot 100 \quad (1)$$

Degradation of the samples were measured every 2 days, after drying the samples and the degradation rate of, each scaffold is calculated according to the formula presented in

Eq. (2) [27].

$$Di = \frac{W_o - W_t}{W_o} \cdot 100 \quad (2)$$

2.2.10. In-vitro drug release and encapsulation efficiency

In vitro release study of drug-loaded nanoparticle-containing scaffolds was performed in PBS. For this 10 mg of each scaffold was placed in Eppendorf tubes and 1 ml of PBS was added. Further, the tubes were placed in a thermal shaker (BIOSAN TS-100, Riga Latvia). Supernatants from each scaffold was testes after 15 mins, 30 min, 60 min, 2 h, 3 h, 4 h, 6 h, 8 h, 12 h, and 24 h of the incubation, and the new portion of PBS was added to each tube. The retention continued until all of the drugs were released. The amount of the drugs within the tested supernatents were measured using UV spectrophotometer (Shimadzu UV-3600, Kyoto, Japan) between 190 and 500 nm wavelength.

2.2.11. In vitro drug release kinetics

To evaluate the drug release kinetics of scaffolds containing drug-loaded nanoparticles, the following mathematical models were used, respectively: Korsmeyer-Peppas (4), zero-order (5), first-order (6), Higuchi (7), and Hixson-Crowell (8) were below, respectively [28].

$$Q = Kt^n \quad (4)$$

$$Q = K_0 t \quad (5)$$

$$In(1 - Q) = -K_1 t \quad (6)$$

$$Q = K_h t^{1/2} \quad (7)$$

$$Q^{1/3} = K_{hc} t \quad (8)$$

In these mathematical models the fractional amount of drug release at time t is represented by the expression Q. For zero-order, first-order, Korsmeyer-Peppas, Higuchi, and Hixson- Crowell models, respectively K0, K1, K, Kh, and Khc, symbolize kinetic constants. The diffusion, which is the indicator of the drug release mechanism, is expressed with

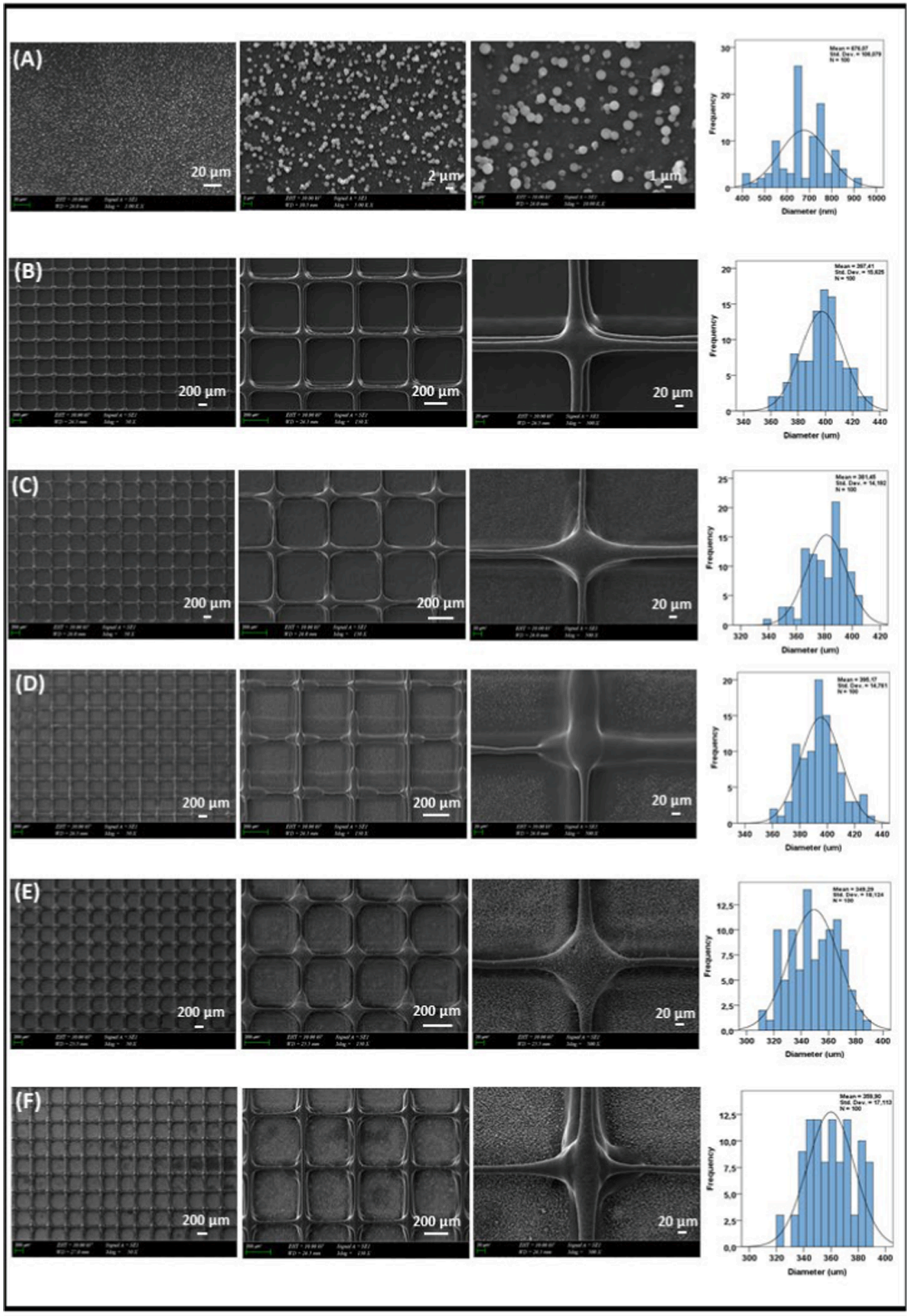

Fig. 2. Morphological structure of layer by layer 3D pure PCL scaffold, pure PVP nanoparticle, and both drug-loaded and non drug-loaded particle-scaffold combining structure. A) PVP nanoparticle B) Pure PCL scaffold C) 7PCL/PVP D) 2PCL/PVP/5PCL E) 7PCL/Tet- PVP F) 2PCL/Tet-PVP/5PCL.

n.

2.2.12. Cell culture studies

To study how cells interact with scaffolds of various compositions and design, the mouse fibroblast cell line was employed. First, scaffolds placed in 96-well plates were sterilized overnight using ultraviolet (UV) light. Next, the scaffolds were incubated for an hour at 37 °C and 5 % CO2 in the growing medium containing DMEM, FBS (10 % v/v), and penicillin/streptomycin (0.1 mg/ml). The extra media was then removed and scaffolds were seeded with fibroblast cells at a density of 5 × 10^3 cells/ml, and further incubated for a week at 37 °C with 5 % CO2. For cross-control, 200 µl of monolayer (2D) cell cultures containing the same number of cells were treated in the same manner. At the end of the first, third, and seventh day, the cytotoxicity of the scaffolds was assessed using a cell viability assay (MTT, Glentham Life Sciences). The absorbance from the MTT dye was examined using an ELISA reader (Perkin Elmer, Enspire) operating at a 560 nm wavelength. The test was run three times, and the average of the outcomes was taken as the final finding.

2.2.12.1. DAPI staining. To assess the fibroblast cells' viability on the scaffolds, DAPI nuclei labeling was used. For this, after first, third, and seventh day the scaffolds were removed from the growth medium and cleaned with PBS. Next, the cell-scaffolds constructs were exposed to 4 % formaldehyde for 30 min at RT and further rewashed with PBS. Each scaffold was stained by adding 1 g/ml DAPI and incubating for 20 min. The scaffolds were then removed from the DAPI solution, sandwiched between two glass slides, and examined using a fluorescence-inverted microscope (Leica).

2.2.12.2. SEM analysis. SEM was used evaluate fibroblasts' cell morphology. After 1, 4, and 7 days, the scaffolds were taken out of the growing media and subjected to 4 % glutaraldehyde in order to preserve the cells on the scaffolds. Further the samples were dehydrated with series of ethanol dillution and dried in the air. As a last step the samples were coated with a gold–palladium sputter and observed using SEM (EVO MA-10, Zeiss).

2.2.13. Statistical analysis

All experiments were carried out at least in triplicates and data are expressed as mean ± standard deviation (SD). The results were evaluated statistically by means of a single-factor ANOVA. A value of $p \leq 0.05$ was considered statistically significant, and additional significance was indicated with $^{**}p < 0.01$ and $^{***}p < 0.001$.

3. Result and discussion

3.1. Morphology of the fabricated scaffolds

When considering the drug release mechanisms, the surface morphology, pore structure, size of the pores within the structure, and shape and size of the particles attached to the scaffold are important parameters, which influence the activity of the scaffolds, when implanted into the tissue. The microporous scaffolds produced from polymers should be compact, possess smooth surfaces, and porosity should be homogeneous with good interconnection between the pores [29]. The pore size of the structure, which will carry the loaded active substance to the target, needs to be appropriate for nutrient and gas transfer, and sufficient for the cells to adhere to the scaffold, and multiply. Moreover, the pore size and pore density support the flexibility, durability, and mechanical stability of the scaffold. 3D printing methods are preferred for obtaining the desired size of pores and their microporosity [30–32].

Obtained SEM results show that the PVP particles of an average size of 676 ± 108 nm were completely spread between and on the scaffolds,

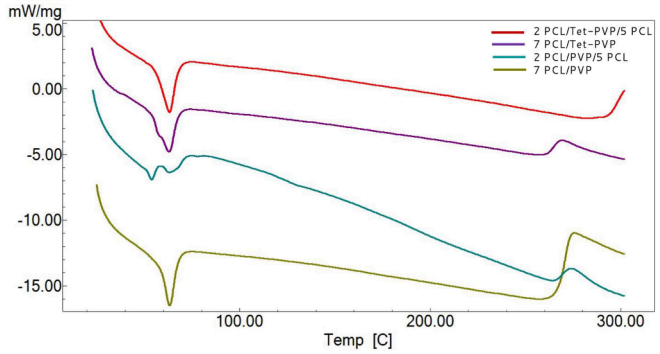

Fig. 3. DSC thermal analysis graphic.

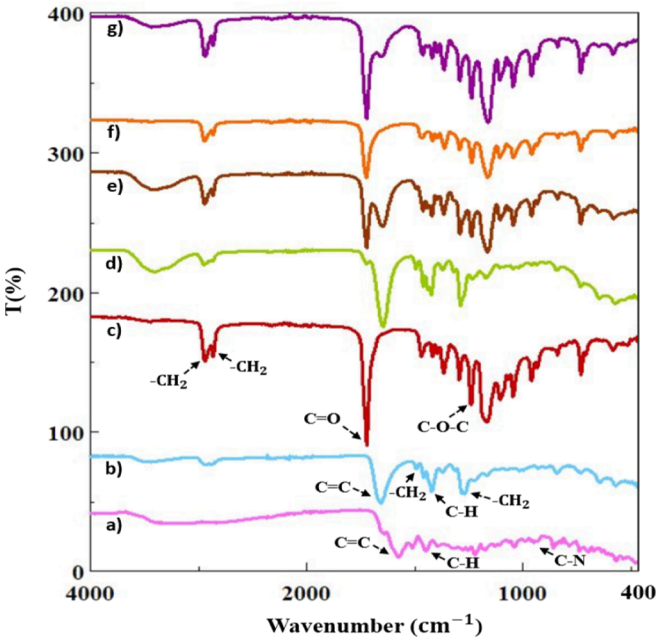

Fig. 4. FTIR spectrums of (a) Tet, (b) PVP, (c) PCL, (d) 7PCL/PVP, (e) 2PCL/PVP/5PCL, (f) 7PCL/Tet-PVP, (g) 2PCL/Tet-PVP/5PCL.

and were homogeneously distributed, regarding of the type of the scaffolds and the addition of Tet (Fig. 2). The size of the pores was recorded as 397 ± 15 µm., 381 ± 14 µm, 385 ± 14 µm, 349 ± 18 µm, and 360 ± 17 µm for 7-layer pure PCL, 7PCL/PVP, 2PCL/PVP/5PCL, 7PCL/Tet-PVP and 2PCL/Tet- PVP/5PCL, respectively. Since the cells are generally 10–20 µm in size, it is advantageous for them to form a tissue-like structure when the pores are larger than 20 µm [33]. One parameter that affects the size of the pores of the scaffold is the diameter of the needle used during 3D printing. The smaller the diameter of the needle, the greater the spacing of the pores in the same size scaffold, which in turn enables more drug-loaded nanoparticles to be placed in the formed pores, thus, the particle-carrying capacity of the scaffold increases.

3.2. Thermal properties of the scaffolds

DSC analysis was applied to evaluate the thermal properties of obtained scaffolds, and the resultant thermograms obtained for 7-7PCL/PVP, 2PCL/PVP/5PCL, 7PCL/Tet-PVP, 2PCL/Tet-PVP/5PCL are shown in Fig. 3. As determined for the PCL scaffold in the study of Wei et al., the PCL polymer has its melting point at 60 °C - 62 °C [34]. According to the study by Kim et al., the melting point of the PVP microparticles was shown to be 160 °C [35]. The melting temperatures of the scaffolds

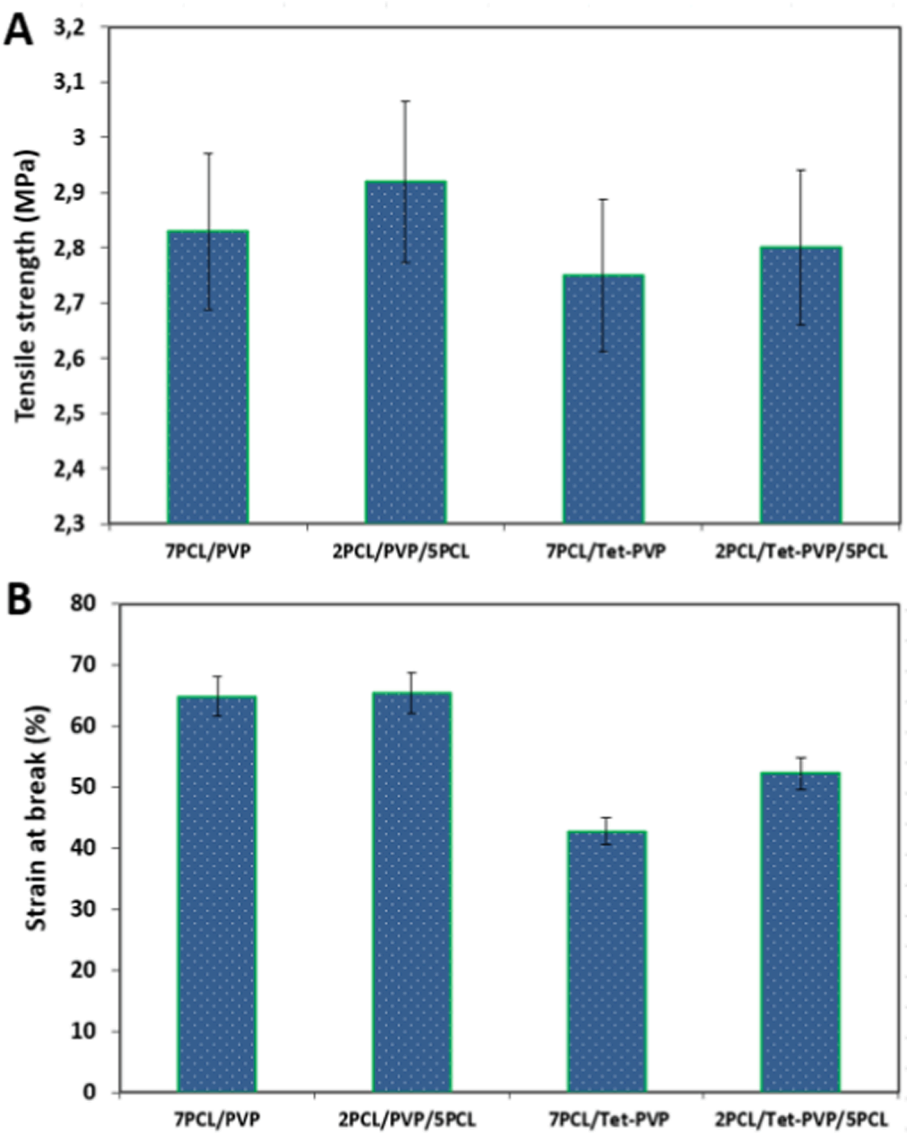

Fig. 5. Tensile strength (a) and the elongation values (b) of 7PCL/PVP, 2PCL/PVP/5PCL, 7PCL/Tet-PVP, and 2PCL/Tet-PVP/5PCL scaffolds.

containing PVP particles sprayed on the 2nd and 7th layer of the PCL scaffold did not differ much compared to the pure PCL scaffold. The melting temperature remained stable. 7-7PCL/PVP, 2PCL/PVP/5PCL, 7PCL/Tet-PVP, 2PCL/Tet-PVP/5PCL groups shows melting point, respectively at 63.31 °C, 63.19 °C, 63 °C and 63.18 °C. The reason for the peaks appearing at values close to the PCL melting point in the combined structures can be explained by the high PCL to PVP ratio, and thus the thermal properties are closer to the ones exhibited by PCL. Since the human body temperature is 37 °C on average [36], the scaffold forming the Tet-loaded drug transport system is resistant to the heat level of the human body.

3.3. Chemical properties of the scaffolds

FTIR analysis was used to determine the chemical interactions and functional groups of the fabricated scaffolds. The absorption peaks of Tet are shown in Fig. 4a and the peak at ~ 1577.4 cm^{-1} corresponds to the C═C stretching. At the peak ~ 1446.3 cm^{-1}, aromatic C—H bending is observed. C—N stretching vibration is visible on the peak at ~ 956.8 cm^{-1}. The presence of a peak at ~ 566.9 cm^{-1} indicates the aromatic out-plane deformation [37]. For PVP, (Fig. 4 b) the sharpest peak is visible at ~ 1654.6 cm^{-1}, and is observed due to C═C vibrational stretching of the amide I, and represents the characteristic group of this polymer. CH2 scissor mode is observed at the peak ~ 1491.6 cm^{-1}. The presence of a peak at ~ 1419.3 cm^{-1} indicates in-plane bending vibration from C—H [38]. The peak indicating the twisting of CH2 is observed at ~ 1282.4 cm^{-1}. In Fig. 4c, the absorption peaks of PCL are shown, and the absorption peaks at ~ 2938.9 cm^{-1} and ~ 2865.7 cm^{-1} correspond to asymmetric and symmetric CH2 stretching, [39]. The peak indicating the C═O carbonyl stretching is observed at ~ 1720.1 cm^{-1}. The peak, which is seen at ~ 1240 cm^{-1} corresponds to C-O-C asymmetric stretching. Fig. 4 d-g present FTIR spectra of 3D-printed scaffolds loaded with PVP and PVP/Tet. The characteristic absorption peaks of the PCL polymer are visible at ~ 2938.9 cm^{-1}, ~2865.7 cm^{-1} and ~ 1240 cm^{-1} were observed for all produced scaffolds. The peaks seen at ~ 1654.6 cm^{-1} (Fig. 4 d and e) are associated with PVP particles. However, it was not observed for the scaffolds with embedded with Tet loaded particles. Although electrospraying with PVP is performed for all particles, adding Tet reduced the transmittance of drug-loaded particles, and caused suppression of the absorption peak of the PVP polymer. As a result, it was concluded that PVP/Tet drug-loaded particles were successfully loaded onto scaffolds and led to intermolecular interactions.

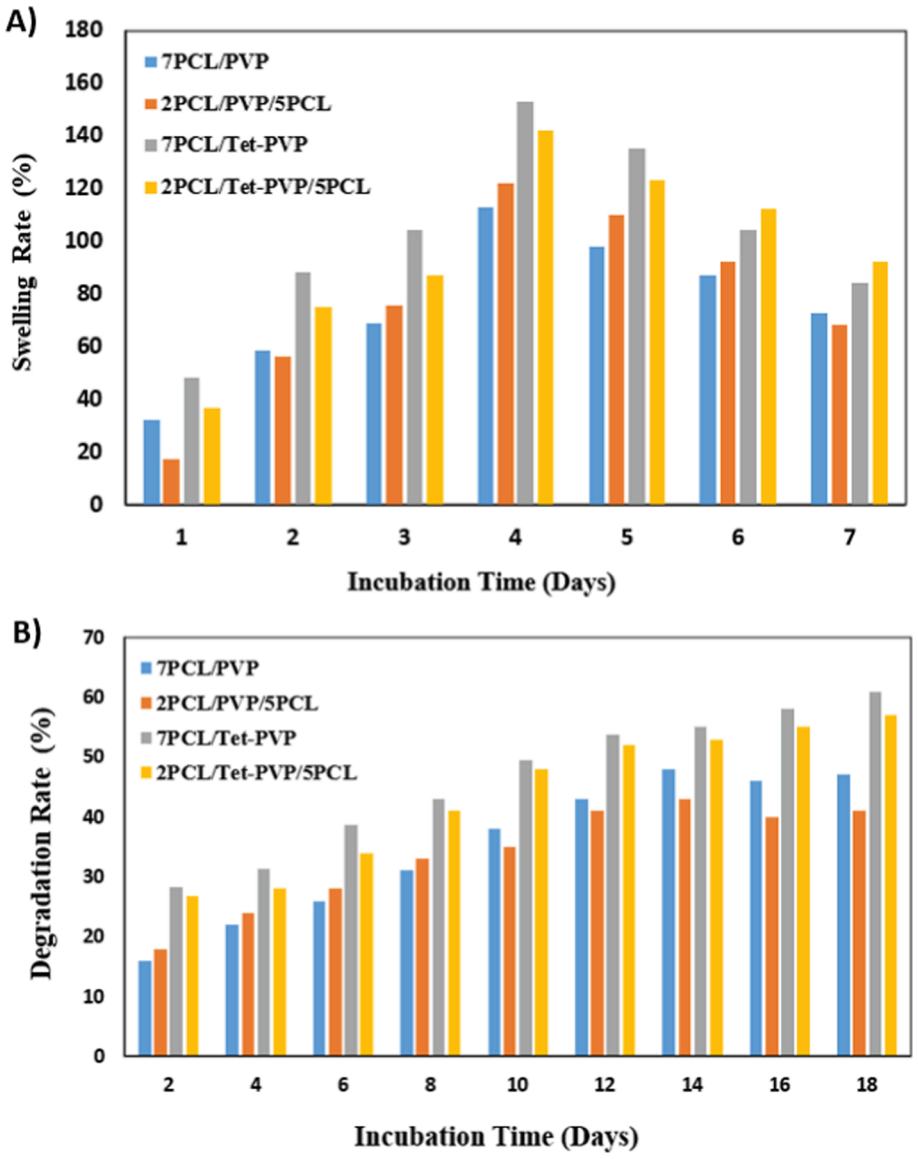

Fig. 6. Water uptake capacity (a) and degradation (b) behaviors of 3D-printed scaffolds.

3.4. Mechanical strength of the scaffolds

In tissue engineering applications, the produced scaffolds need to have appropriate flexibility and mechanical properties. Tissue engineering constructs should not break under the specific load and should keep their structural integrity during the healing process [40,41]. Fig. 5a and 5b represents the tensile strength and elongation and break values of the fabricated scaffolds. The tensile strength of the scaffolds produced for tissue engineering applications can vary between 2–480 MPa depending on the type of the tissue, in which they are attended to be used [42]. Structural changes made by electrospraying of pure PVP particles on different layers in the structures did not cause much change in tensile strength. 7PCL/PVP and 2PCL/PVP/5PCL scaffolds showed a tensile strength of 2.83 ± 0.2 and 2.92 ± 0.1 MPa, respectively, while their elongation values were 64.86 % and 65.45 %. When Tet was added to the particles embedded within the scaffolds the tensile strength of the scaffolds decreased to 2.75 ± 0.4 and 2.8 ± 0.1 MPa for 7PCL/Tet-PVP and 2PCL/Tet-PVP/5PCL, respectively. The elongation of the PVP-Tet-loaded scaffolds was 42.8 % and 52.28 %, respectively. Studies published by Farzamfar et al. also showed that scaffolds' mechanical strength values decrease with the Tet addition [43].

3.5. Swelling and degradation

The water absorption property influences the cell attachment and proliferation on the surface, and transport of nutrients through 3D scaffolds and the swelling capacity allows scaffolds to absorb body fluids [44]. According to the graph presented in Fig. 6a, it can be seen that the scaffolds exhibit a swelling profile until day 4th, and then degradation of their structure occurs. On the 4th day, the swelling rate of 113 % is observed for the 7PCL/PVP, and is lowest compared for other tested scaffolds, and PCL/Tet-PVP has the highest swelling value of 153 %. Parsa et al. stated that the increase in the swelling ratio might be related to the increase in the hydrophilic group from Tet, and therefore it absorbs more water [45]. 2PCL/Tet-PVP/5PCL had a swelling ratio of 142 %, similar to the PCL/Tet-PVP, supporting the fact that the Tet-containing scaffolds absorb more water compared to the non drug-loaded ones.

Degradation is important in terms of the stability of the construct during the cells grow within the scaffolds [46]. The degradation behavior of the produced scaffolds was observed for 18 days, and it was determined that the scaffolds lost weight and started to dissolve over time. According to the 18-day degradation profile in Fig. 6b, 7PCL/Tet-

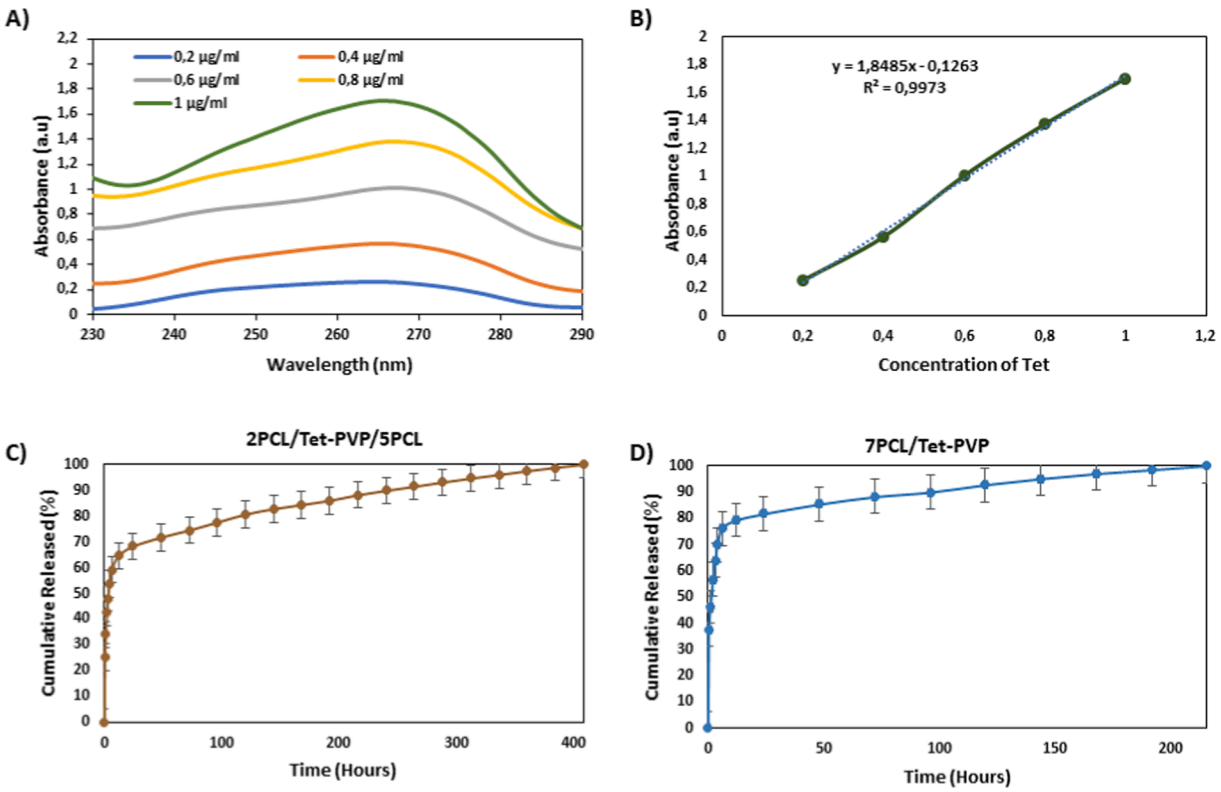

Fig. 7. *In vitro* drug release profiles of Tet from the 3D-printed scaffolds: Absorption spectra of Tet at different concentrations (a), Tet calibration curve (b), Tet release profiles from the 2PCL/Tet-PVP/5PCL (c) and 7PCL/Tet-PVP (d) scaffolds. All the measurements were repeated three times and the errors were less than 5%.

PVP group has the highest degradability with a degradation rate of approximately 60 %. It was observed that the degradation rates of 7PCL/Tet-PVP and 2PCL/Tet-PVP/5PCL scaffolds were higher than the degradation rates of 7PCL/PVP and 2PCL/PVP/5PCL groups in which Tet was not loaded into the particles. Sahafnejad et al. reported that the swelling ratio and degradation time increase as a result of the addition of graphene oxide to the PCL scaffold [47]. Similarly, in this study, it was observed that the addition of Tet to PCL scaffolds increased swelling and degradation rates.

3.6. Drug release and kinetics

In vitro drug release tests were performed in physiological mimicking conditions of living organisms performed at 37 °C at pH 7.4 for 408 h (17 days) to examine the release profiles of Tet from PVP particles embedded in 3D-printed scaffolds with different designs. The absorbance for different concentrations of Tet according to the peak value obtained at 266 nm is plotted in Fig. 7a. The amount of tetracycline released from the scaffolds was investigated by UV spectroscopy using calibration curvespresented in Fig. 7b. When the cumulative release graphs of Tet were examined, it was observed that a burst release of 76.13 % occurred after 6 h for 7PCL/Tet-PVP and of 64.55 % at 12 h for 2PCL/Tet- PVP/5PCL scaffolds, respectively. This result showed that the drug encapsulated between the layers was better protected and released slower than the drug encapsulated on the scaffold's surface. However, the cumulative release obtained for both types of scaffolds also show differences between the release times. The release of Tet from the 7PCL/Tet-PVP scaffold takes 216 h (9 days) to complete, while the release takes up to 408 h (17 days) for the 2PCL/Tet-PVP/5PCL scaffolds (Fig. 7c and 7d). Embeding of the PVP Tet-loaded particles into the interlayer in the produced structures prolonged the release time and provided a more controlled release profile. Given that PCL degrades in a very long time, it is a particularly desirable foundation for long-term drug delivery applications[48]. Turdimuhammad et al. study demonstrated that drug-loaded chitin-lignin (CL) gel exhibited a sustained and controlled release profile after coating with PCL[49]. On the other hand, Susmita et al. study investigated the release profile of alendronate-loaded Mg-doped Hydroxyapatite constructs coated with PCL at different concentrations.. They demonstrated that a higher PCL concentration in coating the slower burst release and longer duration of drug release is observed compared to a lower concentration and no coating[50].

The Zero-order, First-order, Korsmeyer-Peppas, Higuchi, and Hixson-Crowell release models were utilized to explore the release kinetics of Tet from a PVP particles embedded 3D scaffolds. Table 1 shows the reaggregation coefficients (R^2) and kinetic constants of the scaffolds. While the Korsmeyer-Peppas model provides the best fit for the tetracycline loaded 2PCL/Tet-PVP/5PCL scaffolds with higher R2 value, it can be said that it is the First order model for the 7PCL/Tet-PVP scaffolds. (Fig. 8). Also, the drug release mechanism from the polymeric material is determined by the n value (Table 2). The value of $n \geq 0.45$ represents a Fickian diffusion mechanism, between $0.45 < n < 0.89$, a

Table 1
Results of mathematical drug release patterns of 3D-printed scaffolds.

Sample	Korsmeyer-Peppas		Zero-Order		First-Order		Higuchi		Hixson-Crowell	
	R^2	n	R^2	K_0	R^2	K_1	R^2	K_h	R^2	K_{hc}
2PCL/Tet-PVP/5PCL	0,9376	28,429	0,7176	0,1506	0,9298	−0,0034	0,8615	3,4337	0,9017	0,007
7PCL/Tet-PVP	0,7314	26,69	0,4966	0,2467	0,926	−0,0072	0,6624	4,1554	0,841	0,0138

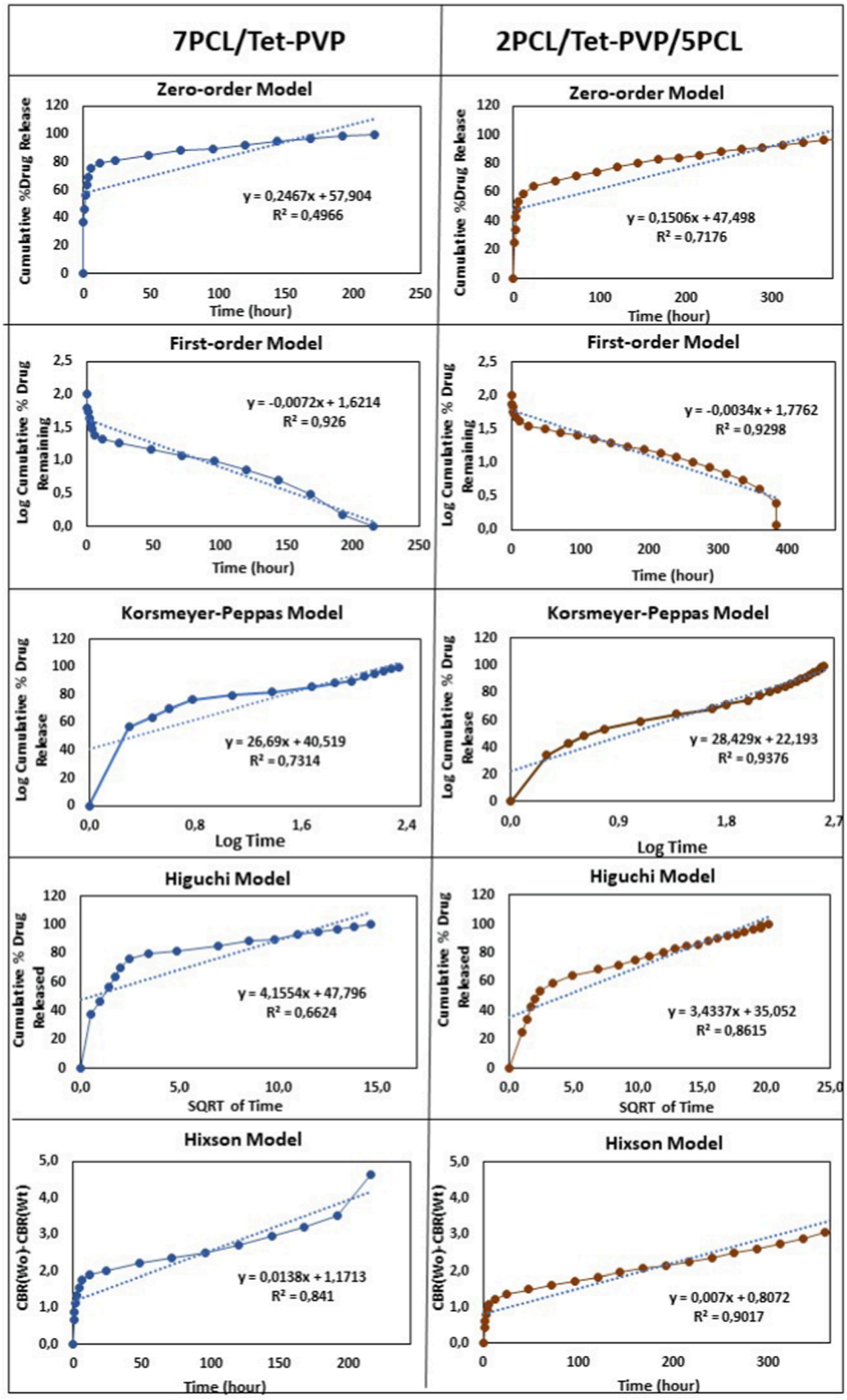

Fig. 8. The kinetic release models of Tetracilin release profiles from the 7PCL/Tet-PVP and 2PCL/Tet-PVP/5PCL scaffolds; Zero-order, First-order, Korsmeyer-Peppas, Higuchi, and Hixson-Crowell models.

Table 2
Transport mechanisms where the "n" value corresponds.

The ranges of n values	Transport mechanisms
$0.45 \leq n$	Fickian diffusion mechanism
$0.45 < n < 0.89$	Non-Fickian transport
$n = 0.89$	Case II (relaxational) transport
$n > 0.89$	Super case II transport

non-Fickian diffusion, at $n = 0.89$ the polymer relaxes, and for $n > 0.89$ a super case II transport [19,51]. Both Tet-loaded scaffolds have an n value greater than 1, suggesting that the drug is released from the scaffolds via super-state II transport.

3.7. Cell viability analysis

The MTT Assay was used to examine the biocompatibility, which is a

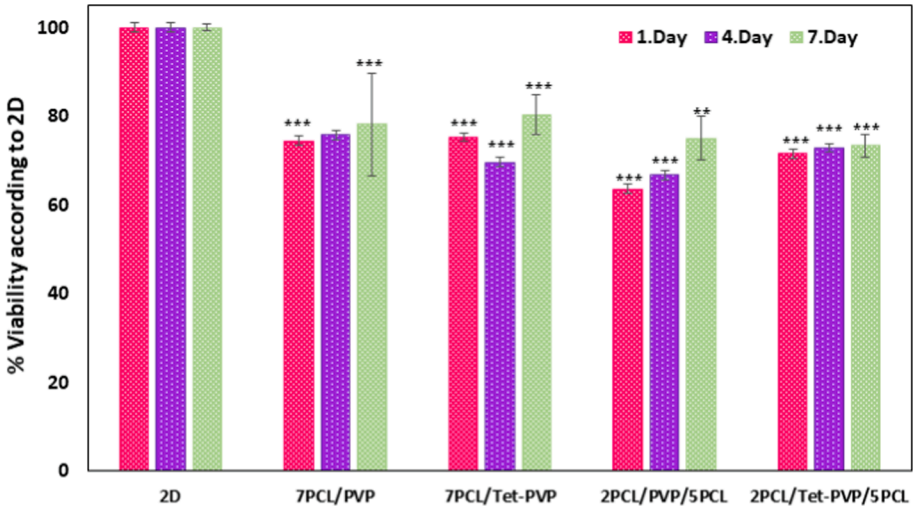

Fig. 9. Cell viability analysis of the scaffolds with their standard deviations (*p < 0,05, **p < 0,01, ***p < 0,001).

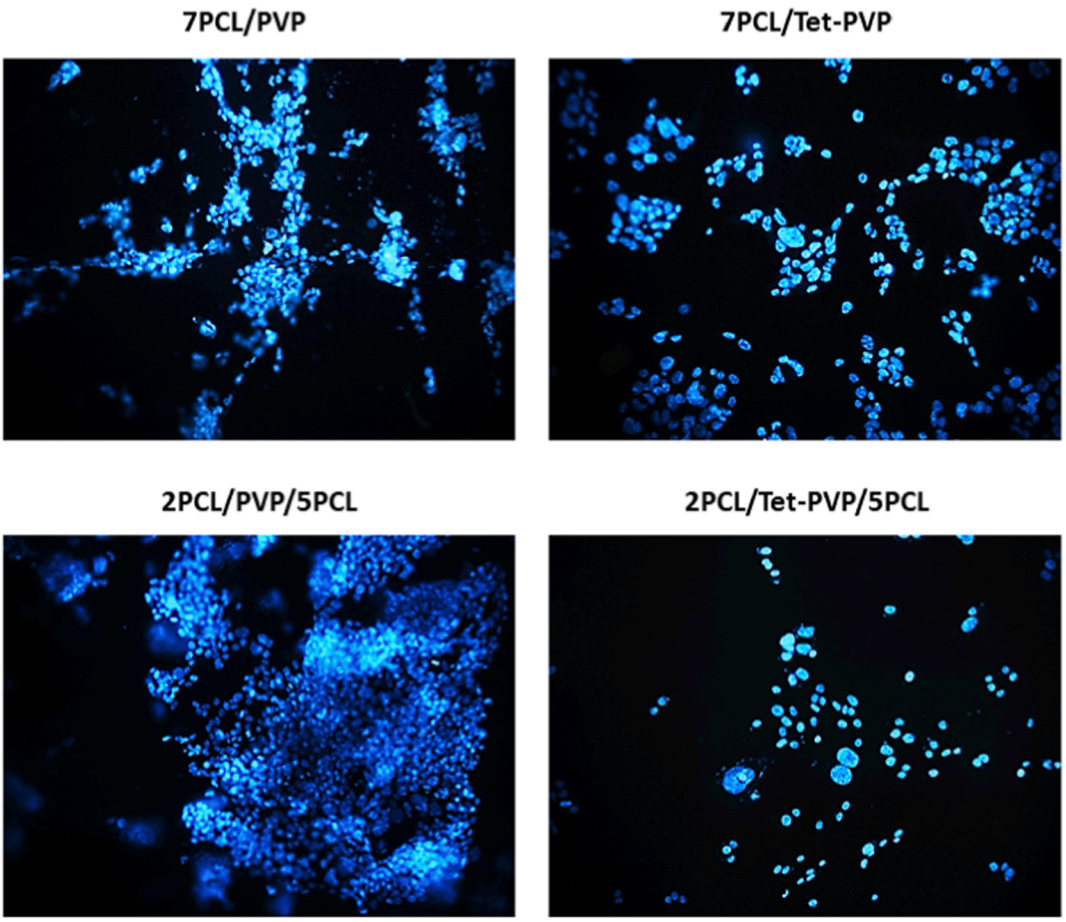

Fig. 10. Fluorescence microscopy images of Fibroblast cells which were nucleus stained with DAPI on scaffolds after 7th days incubation.

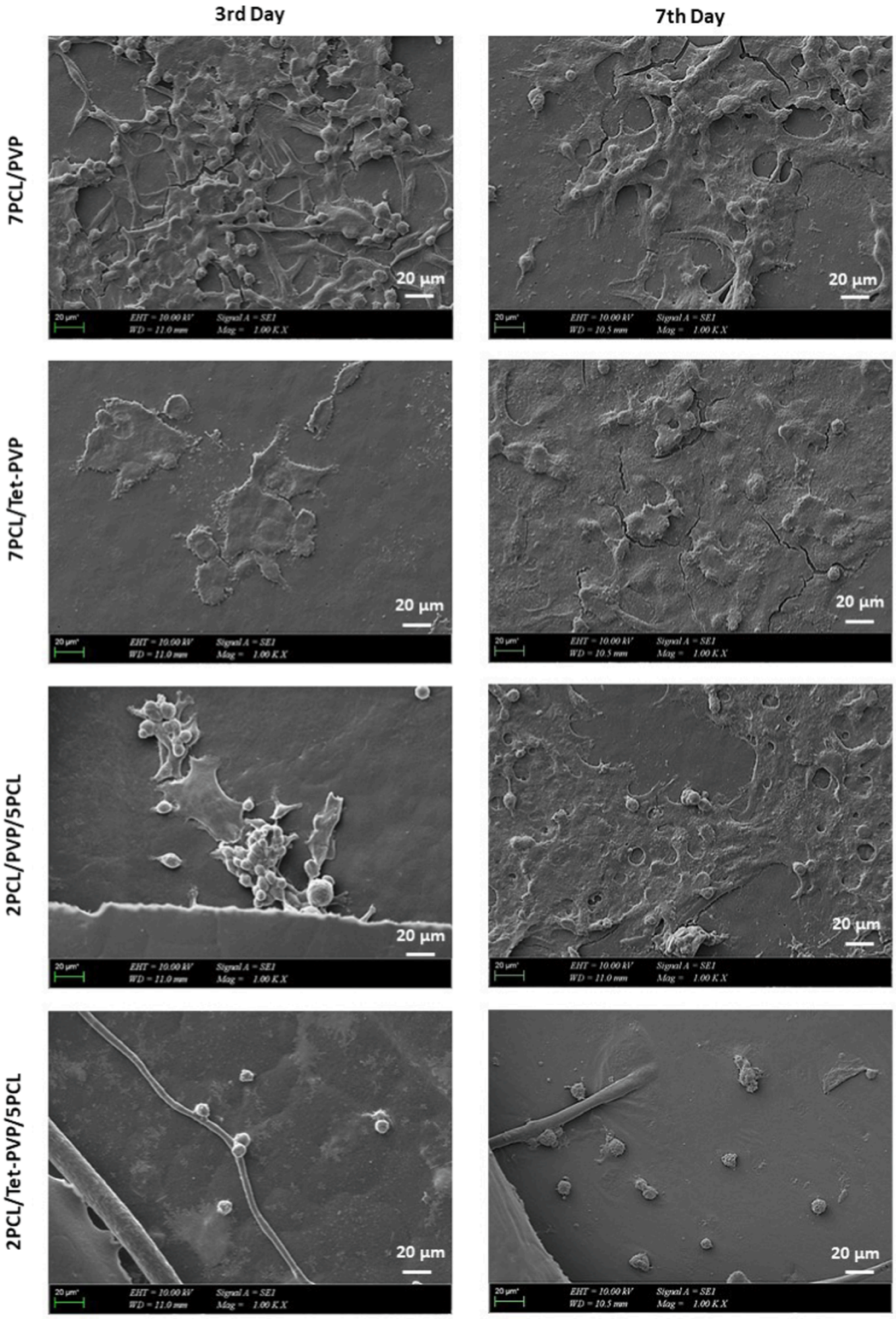

Fig. 11. SEM images of fibroblast cell attachment on the scaffolds after the 3rd-day and 7th-day incubation.

key factor in tissue regenerationusing 3D scaffolds. The biocompatibility of structures is based on some specific criteria, including non-toxicity, strong cell adhesion, proliferation, and differentiation [52]. MTT chromometry assay was performed for 7 days to evaluate cell viability of the cells cultured on the fabricated 3D-printed scaffolds. Compared to the 2D control group, it can be seen (Fig. 9) that the cell viability increased towards the third and seven days of the culture. When all groups are compared among themselves in terms of cell viability, it is observed that they do not show significant differences. It is observed that the change in the production technique of the scaffolds does not cause any effect on cell viability.

As shown in Fig. 10, fluorescent microscopy images were taken to prove the viability of the cells on the scaffolds. After 7 days of incubation a high density of viable cells on the surface of all four scaffolds was

observed. Cell viability was found to be similar on 7PCL/PVP, 7PCL/Tet-PVP, and 2PCL/PVP/5PCL scaffolds, but slightly lower on 2PCL/Tet-PVP/5PCL scaffolds. The cellular aggregates formedon the scaffolds result from the attachment to themicrofibers of the 3D structures of the scffoolds, and it can be obeserved that the cells tend to spread and penetrate the scaffolds.

In addition, cell-material interaction was analyzed by SEM imaging. In Fig. 11, cell moprhology in contact with material is observed for 3 days and 7 days of incubation. The images show that the highest number of spread cells is observed for cells cultured on the 7PCL/PVP scaffolds, and the least on the 2PCL/Tet-PVP/5PCL scaffolds. This states in accordance to the fluorescent imaging results.

4. Conclusions

In this study, 3D porous PCL scaffolds containing pure and Tet-loaded PVP nanoparticles were designed and fabricated using 3D printing and electrospray techniques, and layered porous structures have been obtained. Performed analysis of morphology confirmed that PVP particles were homogeneously distributed on the top or between the layers of the scaffolds completely covering the layers they were sprayed on to. The distance between the pores for 7- layer pure PCL was recorded as 397 ± μm. This distance was measured as 381 ± 14 μm, 385 ± 14 μm, 349 ± 18 μm, and 360 ± 17 μm for 7PCL/PVP, 2PCL/PVP/5PCL, 7PCL/Tet-PVP and 2PCL/Tet-PVP/5PCL, respectively. Structural changes and the addition of Tet did not cause significant difference in tensile strength, however, 2PCL/PVP/5PCL and 2PCL/Tet- PVP/5PCL scaffolds exhibited higher tensile strength due to their structure, while encapsulation particles with Tet decreased both tensile strength and elongation at break of the stractures. Water absorption and degradation results, along with swelling and degradation show an increase of this properties for 7PCL/Tet-PVP and 2PCL/Tet-PVP/5PCL scaffolds compared to the groups without Tet. The drug release was found to be longer and more stable for the 2PCL/Tet-PVP/5PCL scaffolds compared to 7PCL/Tet-PVP scaffold confirming that encapsulation of the drug into the interlayer of the produced structures extended the release time and provided a more controlled release profile. Cell culture findings after 7 days of incubation, revealed that fibroblast cells adhered to and multiplied on the scaffold surface. All scaffolds exhibited an appropriate level of biocompatibility and no harmful effects. Considering obtained results, the design of hydrophobic PCL scaffolds containing a hydrophilic drug inside of PVP particles using 3D printing and electrospray techniques provide a potential drug delivering scaffolds for the development of a new functional scaffolds.

Declaration of competing interest

The authors declare that they have no known competing financial interests or personal relationships that could have appeared to influence the work reported in this paper.

Data availability

The data that has been used is confidential.

References

[1] A. Siddiqui, N. Farhat, S.S. Bucs, R.V. Linares, C. Picioreanu, J.C. Kruithof, M.C. M. Van Loosdrecht, J. Kidwell, J.S. Vrouwenvelder, Development and characterization of 3D-printed feed spacers for spiral wound membrane systems, Water Res. 91 (2016) 55–67, https://doi.org/10.1016/J.WATRES.2015.12.052.

[2] D. Yadav, R.K. Garg, A. Ahlawat, D. Chhabra, 3D printable biomaterials for orthopedic implants: Solution for sustainable and circular economy, Resour. Policy. 68 (2020), 101767, https://doi.org/10.1016/J.RESOURPOL.2020.101767.

[3] T.P. Kraehenbuehl, R. Langer, L.S. Ferreira, Three-dimensional biomaterials for the study of human pluripotent stem cells, Nat. Methods. 8 (2011) 731–736, https://doi.org/10.1038/nmeth.1671.

[4] S.E. Moulton, G.G. Wallace, 3-dimensional (3D) fabricated polymer based drug delivery systems, J. Control. Release. 193 (2014) 27–34, https://doi.org/10.1016/J.JCONREL.2014.07.005.

[5] B. Baumann, T. Jungst, S. Stichler, S. Feineis, O. Wiltschka, M. Kuhlmann, M. Lindén, J. Groll, Control of Nanoparticle Release Kinetics from 3D Printed Hydrogel Scaffolds, Angew. Chemie Int. Ed. 56 (2017) 4623–4628, https://doi.org/10.1002/ANIE.201700153.

[6] I.R. Calori, G. Braga, P. da C.C. de Jesus, H. Bi, A.C. Tedesco, Polymer scaffolds as drug delivery systems, Eur. Polym. J. 129 (2020). https://doi.org/10.1016/j.eurpolymj.2020.109621.

[7] M.P. Figueiredo, G. Layrac, A. Hébraud, L. Limousy, J. Brendle, G. Schlatter, V.R. L. Constantino, Design of 3D multi-layered electrospun membranes embedding iron-based layered double hydroxide for drug storage and control of sustained release, Eur. Polym. J. 131 (2020), https://doi.org/10.1016/j.eurpolymj.2020.109675.

[8] W. Shi, M. Sun, X. Hu, B. Ren, J. Cheng, C. Li, X. Duan, X. Fu, J. Zhang, H. Chen, Y. Ao, W. Shi, X. Hu, B. Ren, J. Cheng, C. Li, X. Duan, X. Fu, J. Zhang, Y. Ao, M. Sun, H. Chen, Structurally and Functionally Optimized Silk-Fibroin–Gelatin Scaffold Using 3D Printing to Repair Cartilage Injury In Vitro and In Vivo, Adv. Mater. 29 (2017) 1701089, https://doi.org/10.1002/ADMA.201701089.

[9] E. Michalova, PNovotna, J. Schlegelova, Tetracyclines in veterinary medicine and bacterial resistance to them, Vet. Med. (Praha). 49 (2012) 79–100. https://doi.org/10.17221/5681-VETMED.

[10] M.C. Roberts, Tetracycline therapy: Update, Clin. Infect. Dis. 36 (2003) 462–467, https://doi.org/10.1086/367622.

[11] I. Chopra, M. Roberts, Tetracycline Antibiotics: Mode of Action, Applications, Molecular Biology, and Epidemiology of Bacterial Resistance, Microbiol. Mol. Biol. Rev. 65 (2001) 232–260, https://doi.org/10.1128/mmbr.65.2.232-260.2001.

[12] K.E. Nelson, S. Levin, H.W. Spies, M.H. Lepper, Treatment of Hemophilus injluenzae Meningitis: A Comparison of Chloramphenicol and Tetracycline, J. Infect. Dis. 125 (1972) 459–465, https://doi.org/10.1093/infdis/125.5.459.

[13] M.C. Roberts, Tetracycline resistance determinants: Mechanisms of action, regulation of expression, genetic mobility, and distribution, FEMS Microbiol. Rev. 19 (1996) 1–24, https://doi.org/10.1016/0168-6445(96)00021-6.

[14] D.C. Mabey, A.W. Solomon, A. Foster, Trachoma, Lancet. 362 (2003) 223–229, https://doi.org/10.1016/S0140-6736(03)13914-1.

[15] K.J. Adcock, S. Reddy, O.A. Okubadejo, D. Montefiore, Trimethoprim-sulphamethoxazole in pertussis: comparison with tetracycline, Arch. Dis. Child. 47 (1972) 311–313, https://doi.org/10.1136/adc.47.252.311.

[16] H.W. Spies, K.E. Nelson, S. Levin, M.H. Lepper, Treatment of hemophilus influenzae meningitis: A comparison of chloramphenicol and tetracycline, J. Infect. Dis. 125 (1972) 459–465, https://doi.org/10.1093/infdis/125.5.459.

[17] B.M. Jones, I. Geary, M.E. Lee, B.I. Duerden, Comparison of the in vitro activities of fenticonazole, other imidazoles, metronidazole, and tetracycline against organisms associated with bacterial vaginosis and skin infections, Antimicrob. Agents Chemother. 33 (1989) 970–972, https://doi.org/10.1128/AAC.33.6.970.

[18] M.M. Rubenstein, The Treatment of Acute Otitis Media in Children, Am. J. Dis. Child. 109 (1965) 308, https://doi.org/10.1001/archpedi.1965.02090020310008.

[19] E. Saylam, Y. Akkaya, E. Ilhan, S. Cesur, E. Guler, A. Sahin, M.E. Cam, N. Ekren, F. N. Oktar, O. Gunduz, D. Ficai, A. Ficai, Levodopa-loaded 3d-printed poly (Lactic) acid/chitosan neural tissue scaffold as a promising drug delivery system for the treatment of parkinson's disease, Appl. Sci. (2021), https://doi.org/10.3390/app112210727.

[20] M. Zamani, M.P. Prabhakaran, S. Ramakrishna, Advances in drug delivery via electrospun and electrosprayed nanomaterials, Int. J. Nanomedicine. 8 (2013) 2997–3017, https://doi.org/10.2147/IJN.S43575.

[21] M.E. Tasci, B. Dede, E. Tabak, A. Gur, R.B. Sulutas, S. Cesur, E. Ilhan, C.C. Lin, P. Paik, D. Ficai, A. Ficai, O. Gunduz, Production, optimization and characterization of polylactic acid microparticles using electrospray with porous structure, Appl. Sci. (2021), https://doi.org/10.3390/app11115090.

[22] K. Chhouk, W. Diono, H. Kanda, M. Goto, Micronization for enhancement of curcumin dissolution via electrospraying technique, ChemEngineering. 2 (2018) 1–10, https://doi.org/10.3390/CHEMENGINEERING2040060.

[23] L.R. Fitzpatrick, T. Woldemariam, Small-Molecule Drugs for the Treatment of Inflammatory Bowel Disease, Compr. Med. Chem. III (5–8) (2017) 495–510, https://doi.org/10.1016/B978-0-12-409547-2.12404-7.

[24] M. Guastaferro, L. Baldino, S. Cardea, E. Reverchon, Supercritical CO2 assisted electrospray of PVP-Rutin mixtures using a liquid collector, J. Supercrit. Fluids. 188 (2022), 105684, https://doi.org/10.1016/J.SUPFLU.2022.105684.

[25] Y. Xu, J. Zhao, Z. Zhang, J. Zhang, M. Huang, S. Wang, P. Xie, Preparation of electrospray ALG/PDA-PVP nanocomposites and their application in cancer therapy †, This, J. Is Cite This Soft Matter. 16 (2020) 132, https://doi.org/10.1039/c9sm01584a.

[26] P.A. Rose, P.K. Praseetha, M. Bhagat, P. Alexander, S. Abdeen, M. Chavali, Drug embedded PVP coated magnetic nanoparticles for targeted killing of breast cancer cells, Technol. Cancer Res. Treat. 12 (2013) 463–472, https://doi.org/10.7785/tcrt.2012.500333.

[27] S.N. Alhosseini, F. Moztarzadeh, M. Mozafari, S. Asgari, M. Dodel, A. Samadikuchaksaraei, S. Kargozar, N. Jalali, Synthesis and characterization of electrospun polyvinyl alcohol nanofibrous scaffolds modified by blending with chitosan for neural tissue engineering, Int. J. Nanomedicine. (2012).

[28] M.E. Cam, B. Ertas, H. Alenezi, A.N. Hazar-Yavuz, S. Cesur, G.S. Ozcan, C. Ekentok, E. Guler, C. Katsakouli, Z. Demirbas, D. Akakin, M.S. Eroglu, L. Kabasakal, O. Gunduz, M. Edirisinghe, Accelerated diabetic wound healing by topical application of combination oral antidiabetic agents-loaded nanofibrous scaffolds:

An in vitro and in vivo evaluation study, Mater. Sci. Eng. c. (2021), https://doi.org/10.1016/j.msec.2020.111586.
[29] P. Thangavel, B. Ramachandran, V. Muthuvijayan, Fabrication of chitosan/gallic acid 3D microporous scaffold for tissue engineering applications, J. Biomed. Mater. Res. - Part B Appl. Biomater. 104 (2016) 750–760, https://doi.org/10.1002/jbm.b.33603.
[30] S. Harmanci, A. Dutta, S. Cesur, A. Sahin, O. Gunduz, D.M. Kalaskar, C. B. Ustundag, Production of 3D Printed Bi-Layer and Tri-Layer Sandwich Scaffolds with Polycaprolactone and Poly (vinyl alcohol)-Metformin towards Diabetic Wound Healing, Polymers (basel). 14 (2022), https://doi.org/10.3390/polym14235306.
[31] X. He, W. Li, S. Liu, Y. Li, Y. Chen, N. Dan, W. Dan, M. Zhu, Fabrication of high-strength, flexible, porous collagen-based scaffolds to promote tissue regeneration, Mater. Today Bio. 16 (2022), https://doi.org/10.1016/j.mtbio.2022.100376.
[32] G. Turnbull, J. Clarke, F. Picard, P. Riches, L. Jia, F. Han, B. Li, W. Shu, 3D bioactive composite scaffolds for bone tissue engineering, Bioact. Mater. 3 (2018) 278–314, https://doi.org/10.1016/j.bioactmat.2017.10.001.
[33] J. Hou, L. Chen, Z. Liu, J. Li, J. Yang, A. Zhong, M. Zhou, Y. Sun, L. Guo, Y. Yang, J. Sun, Z. Wang, Sustained release of N-acetylcysteine by sandwich structured polycaprolactone/collagen scaffolds for wound healing, J. Biomed. Mater. Res. - Part a. (2019) 1414–1424, https://doi.org/10.1002/jbm.a.36656.
[34] L. Wei, H. Chang, Y. Wang, S. Hsu, L. Dai, K. Fu, A Gelatin/Collagen/Polycaprolactone Scaffold for Skin Regeneration (2022) 1–15.
[35] W. Kim, J.S. Kim, H.G. Choi, S.G. Jin, C.W. Cho, Novel ezetimibe-loaded fibrous microparticles for enhanced solubility and oral bioavailability by electrospray technique, J. Drug Deliv. Sci. Technol. 66 (2021), 102877, https://doi.org/10.1016/j.jddst.2021.102877.
[36] G. Russo, G. Lamberti, V. Ponte, D. Melillo, I. Industriale, Electrospinning of Drug-Loaded Polymer Systems : Preparation and Drug Release (2011) 18–20, https://doi.org/10.1002/app.
[37] M.K. Trivedi, S. Patil, H. Shettigar, K. Bairwa, M.K. Trivedi, S. Patil, H. Shettigar, K. Bairwa, S.J. Spec-, A. Acta, Spectroscopic Characterization of Chloramphenicol and Tetracycline : An Impact of Biofield Treatment To cite this version : HAL Id : hal-01376485 Pharmaceutica Spectroscopic Characterization of Chloramphenicol and Tetracycline : An Impact of Biofield Trea, 6 (2016) 0–5. https://doi.org/10.4172/21532435.1000395.
[38] H.D. López-Calderón, H. Avilés-Arnaut, L.J. Galán-Wong, V. Almaguer-Cantú, J. R. Laguna-Camacho, C. Calderón-Ramón, J.E. Escalante-Martínez, K. Arévalo-Niño, Electrospun Polyvinylpyrrolidone-Gelatin and Cellulose Acetate Bi-Layer Scaffold Loaded with Gentamicin as Possible Wound Dressing, Polymers (basel). 12 (2020) E2311, https://doi.org/10.3390/polym12102311.
[39] M.S. Izgordu, E.I. Uzgur, S. Ulag, A. Sahin, B. Karademir Yilmaz, B. Kilic, N. Ekren, F.N. Oktar, O. Gunduz, Investigation of 3D-Printed Polycaprolactone-/Polyvinylpyrrolidone-Based Constructs, Cartilage. 13 (2020), https://doi.org/10.1177/1947603519897302, 626S-635S.
[40] Z. Zarekhalili, S.H. Bahrami, M. Ranjbar-Mohammadi, P.B. Milan, Fabrication and characterization of PVA/Gum tragacanth/PCL hybrid nanofibrous scaffolds for skin substitutes, Int. J. Biol. Macromol. 94 (2017) 679–690, https://doi.org/10.1016/j.ijbiomac.2016.10.042.
[41] P. Szymczyk-Ziółkowska, M.B. Łabowska, J. Detyna, I. Michalak, P. Gruber, A review of fabrication polymer scaffolds for biomedical applications using additive manufacturing techniques, Biocybern, Biomed. Eng. 40 (2020) 624–638, https://doi.org/10.1016/j.bbe.2020.01.015.
[42] S. Ustunel, M.E. Prévôt, G.A.R. Rohaley, C.R. Webb, B. Yavitt, G. Freychet, M. Zhernenkov, R. Pindak, E. Schaible, C. Zhu, T. Hegmann, R.J. Clements, E. Hegmann, Mechanically tunable elastomer and cellulose nanocrystal composites as scaffolds for in vitro cell studies, Mater. Adv. 2 (2021) 464–476, https://doi.org/10.1039/D0MA00676A.
[43] S. Farzamfar, M. Naseri-Nosar, H. Sahrapeyma, A. Ehterami, A. Goodarzi, M. Rahmati, G. Lakalayeh, S. Ghorbani, A. Vaez, M. Salehi, Tetracycline hydrochloride- containing poly (ε-caprolactone)/poly lactic acid scaffold for bone tissue engineering application: in vitro and in vivo study, Int. J. Polym. Mater. Polym. Biomater. 68 (2018) 1–8, https://doi.org/10.1080/00914037.2018.1466133.
[44] T. Pan, W. Song, X. Cao, Y. Wang, 3D Bioplotting of Gelatin/Alginate Scaffolds for Tissue Engineering: Influence of Crosslinking Degree and Pore Architecture on Physicochemical Properties, J. Mater. Sci. Technol. 32 (2016) 889–900, https://doi.org/10.1016/j.jmst.2016.01.007.
[45] P. Parsa, A. Paydayesh, S.M. Davachi, Investigating the effect of tetracycline addition on nanocomposite hydrogels based on polyvinyl alcohol and chitosan nanoparticles for specific medical applications, Int. J. Biol. Macromol. 121 (2019) 1061–1069, https://doi.org/10.1016/j.ijbiomac.2018.10.074.
[46] T. Arslan Tut, S. Cesur, E. Ilhan, A. Sahin, O. Samet Yildirim, O. Gunduz, Gentamicin-loaded Polyvinyl alcohol/Whey protein isolate/Hydroxyapatite 3D Composite Scaffolds with Drug Delivery Capability for Bone Tissue Engineering Applications, Eur. Polym. J. (2022), 111580, https://doi.org/10.1016/j.eurpolymj.2022.111580.
[47] I. Sahafnejad-Mohammadi, S. Rahmati, N. Najmoddin, M. Bodaghi, Biomimetic Polycaprolactone-Graphene Oxide Composites for 3D Printing Bone Scaffolds, Macromol. Mater. Eng. n/a (n.d.) 2200558. https://doi.org/https://doi.org/10.1002/mame.202200558.
[48] K. Miller, J.E. Hsu, L.J. Soslowsky, 6.618 - Materials in Tendon and Ligament Repair, in: P. Ducheyne (Ed.), Compr. Biomater., Elsevier, Oxford, 2011: pp. 257–279. https://doi.org/https://doi.org/10.1016/B978-0-08-055294-1.00218-X.
[49] T. Abdullah, K. Gauthaman, A. Mostafavi, A. Alshahrie, N. Salah, P. Morganti, A. Chianese, A. Tamayol, A. Memic, Sustainable drug release from polycaprolactone coated chitin-lignin gel fibrous scaffolds, Sci. Rep. 10 (2020) 20428, https://doi.org/10.1038/s41598-020-76971-w.
[50] S. Bose, A.A. Vu, K. Emshadi, A. Bandyopadhyay, Effects of polycaprolactone on alendronate drug release from Mg-doped hydroxyapatite coating on titanium, Mater. Sci. Eng. c. Mater. Biol. Appl. 88 (2018) 166–171, https://doi.org/10.1016/j.msec.2018.02.019.
[51] S. Erzengin, E. Guler, E. Eser, E.B. Polat, O. Gunduz, M.E. Cam, In vitro and in vivo evaluation of 3D printed sodium alginate/polyethylene glycol scaffolds for sublingual delivery of insulin: Preparation, characterization, and pharmacokinetics, Int. J. Biol. Macromol. 204 (2022) 429–440, https://doi.org/10.1016/j.ijbiomac.2022.02.030.
[52] E. Ilhan, S. Ulag, A. Sahin, B.K. Yilmaz, N. Ekren, O. Kilic, M. Sengor, D. M. Kalaskar, F.N. Oktar, O. Gunduz, Fabrication of tissue-engineered tympanic membrane patches using 3D-Printing technology, J. Mech. Behav. Biomed. Mater. 114 (2020), 104219, https://doi.org/10.1016/j.jmbbm.2020.104219.